(4)

TECHNICAL REPORT BRL-TR-2994

BRL

AD-A208 122

COMPUTATION OF THE ROLL CHARACTERISTICS OF SEVERAL FIN DESIGNS FOR A LONG ROD PENETRATOR

PAUL WEINACHT

MAY 1989

U.S. ARMY LABORATORY COMMAND

BALLISTIC RESEARCH LABORATORY
ABERDEEN PROVING GROUND, MARYLAND

049

UNCLASSIFIED

SECURITY CLASSIFICATION OF THIS PAGE

REPORT DOCUMENTATION PAGE

Form Approved OMB No. 0704-0188

1a. REPORT SECURITY CLASSIFICATION: UNCLASSIFIED	1b. RESTRICTIVE MARKINGS
2a. SECURITY CLASSIFICATION AUTHORITY	3. DISTRIBUTION/AVAILABILITY OF REPORT: Approved for public release, distribution unlimited.
2b. DECLASSIFICATION/DOWNGRADING SCHEDULE	
4. PERFORMING ORGANIZATION REPORT NUMBER(S): BRL-TR-2994	5. MONITORING ORGANIZATION REPORT NUMBER(S)
6a. NAME OF PERFORMING ORGANIZATION: U.S. Army Ballistic Research Laboratory; 6b. OFFICE SYMBOL (If applicable): SLCBR-LF	7a. NAME OF MONITORING ORGANIZATION
6c. ADDRESS (City, State, and ZIP Code): Aberdeen Proving Ground, Maryland 21005-5066	7b. ADDRESS (City, State, and ZIP Code)
8a. NAME OF FUNDING/SPONSORING ORGANIZATION; 8b. OFFICE SYMBOL (If applicable)	9. PROCUREMENT INSTRUMENT IDENTIFICATION NUMBER
8c. ADDRESS (City, State, and ZIP Code)	10. SOURCE OF FUNDING NUMBERS: PROGRAM ELEMENT NO. 62618A; PROJECT NO. 1L162618AH80; TASK NO. 00; WORK UNIT ACCESSION NO. 001 AJ
11. TITLE (Include Security Classification): COMPUTATION OF THE ROLL CHARACTERISTICS SEVERAL FIN DESIGNS FOR A LONG ROD PENETRATOR	
12. PERSONAL AUTHOR(S): WEINACHT, PAUL	
13a. TYPE OF REPORT: Technical Report; 13b. TIME COVERED: FROM _____ TO _____; 14. DATE OF REPORT (Year, Month, Day); 15. PAGE COUNT	
16. SUPPLEMENTARY NOTATION	

17. COSATI CODES			18. SUBJECT TERMS (Continue on reverse if necessary and identify by block number)
FIELD	GROUP	SUB-GROUP	
01	01		Parabolized Navier-Stokes, Finned Projectiles, Roll Characteristics, Roll Damping, Kinetic Energy Projectiles
20	04		

19. ABSTRACT (Continue on reverse if necessary and identify by block number)

A recently developed computational technique has been applied to compute the aerodynamic roll characteristics of three proposed fin designs for a high length to diameter ratio kinetic energy projectile. These aerodynamic parameters include the roll producing moment, the roll damping moment, and the equilibrium spin rate, defined as the spin rate for which the net roll moment is zero. These aerodynamic parameters have been determined by computing the flow field about the projectile using the Parabolized Navier-Stokes computational approach. Estimates of these parameters have also been obtained using engineering approaches. Comparisons between the computational results and range measurements provide validation of the computational approach.

20. DISTRIBUTION/AVAILABILITY OF ABSTRACT: ☒ UNCLASSIFIED/UNLIMITED ☐ SAME AS RPT. ☐ DTIC USERS	21. ABSTRACT SECURITY CLASSIFICATION: UNCLASSIFIED
22a. NAME OF RESPONSIBLE INDIVIDUAL: Paul Weinacht	22b. TELEPHONE (Include Area Code): (301) 278-4280; 22c. OFFICE SYMBOL: SLCBR-LF-C

DD Form 1473, JUN 86 *Previous editions are obsolete.* SECURITY CLASSIFICATION OF THIS PAGE

Table of Contents

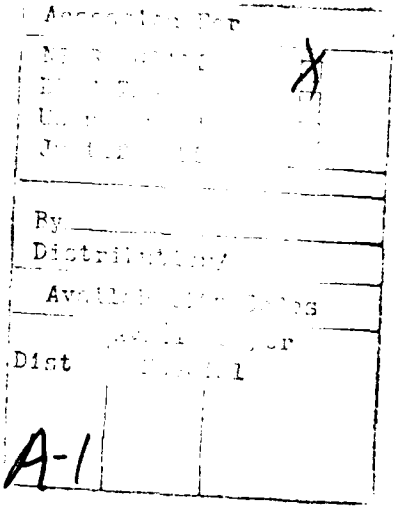

List of Figures

I. INTRODUCTION

A recently developed computational technique[1] has been applied to compute the aerodynamic roll characteristics of three proposed fin designs for a high length-to-diameter ratio (L/D) kinetic energy (KE) projectile. These aerodynamic parameters include the roll producing moment, the roll damping moment, and the equilibrium spin rate, defined as the spin rate for which the net roll moment is zero. These aerodynamic parameters have been determined by computing the flow field about the projectile using the Parabolized Navier-Stokes computational approach. Estimates of these parameters have also been obtained using engineering approaches.

Schematics of the first two fin designs are shown in Figures 1 and 2. Both of these fin designs have beveled trailing edges to produce roll. The third fin design is nearly identical to the second fin design except that the fins are canted with respect to the projectile body as shown in Figure 3. The third fin design also has no beveled trailing edge, since the roll is produced by the fin cant. The fin geometries of the first two fins were completely specified by the projectile designer. For the third design, the fin cant angle was not specified before the start of the computations, but rather the computational approach was used to determine the appropriate cant angle to yield a range of spin rate specified by the projectile designer. It is believed that this represents the first application of computational aerodynamics within the US Army ballistics community where aspects of the projectile geometry were determined using a three-dimensional Navier-Stokes computational approach.

To date, range firings of the second fin design have been performed and roll trajectories have been measured. The roll producing and roll damping moment coefficients and the equilibrium spin rate have been reduced from the range measurements and comparisons are made with the computational results.

In this report, the equation of motion for a projectile undergoing pure rolling moment is briefly discussed in the next section. The computational and engineering estimation techniques used to predict the roll characteristics are briefly presented in the following two sections. Presentation and discussion of the results obtained by applying these techniques to the three fin designs of interest is made in Section V.

II. THE ROLL EQUATION

Aero-ballisticians describe the spin history of the projectile in terms of the following ordinary differential equation[2];

$$I\frac{dp}{dt} = \frac{1}{2}\rho_\infty a_\infty^2 M_\infty^2 D S_{ref} C_l \tag{1}$$

where p is the spin rate, t is time, I is the transverse moment of inertia, C_l is the net aerodynamic roll moment coefficient acting on the projectile, and ρ_∞, a_∞, M_∞, D, and S_{ref} are respectively the reference density, speed of sound, Mach number, diameter, and area.

The net aerodynamic roll moment is composed of two components, the roll producing

moment and the roll damping moment. The roll producing moment, which induces spin on the projectile, results from the aerodynamic loads produced by either the machined asymmetries in the fin geometry or by the fin cant, while the roll damping contribution consists of pressure and viscous forces that oppose the spin. The relationship of these contributions to the net aerodynamic roll moment is expressed below in non-dimensional form,

$$C_l = C_{l_o} + C_{l_p}\frac{pD}{V} \tag{2}$$

where C_{l_o} is the roll producing moment coefficient, C_{l_p} is the roll damping moment coefficient and $\frac{pD}{V}$ is the non-dimensional spin rate. The roll damping coefficient will differ in sign with the roll producing moment coefficient and if the direction of positive roll moment is in the same direction as positive spin, the roll damping coefficient will have a negative value.

For the case of the canted fin, the roll producing moment usually shows a linear variation with cant angle as expressed below,

$$C_{l_o} = C_{l_\delta}\delta \tag{3}$$

where δ is the fin cant angle and C_{l_δ} is the slope of the roll producing moment coefficient with respect to cant angle.

As is suggested in Equation 2, the roll producing moment can be obtained by computing the net aerodynamic roll moment at zero spin rate, while the roll damping moment is obtained by computing the net aerodynamic roll moment on the projectile at a fixed spin rate, subtracting the roll producing moment from it and dividing by the spin rate. The equilibrium spin rate, which occurs when the net aerodynamic roll moment is zero, is obtained by determining the absolute value of the ratio of the the roll producing moment to the roll damping moment.

III. COMPUTATIONAL APPROACH

Computation of the viscous flow field about the finned projectile configurations was accomplished by solving the thin-layer Navier-Stokes equations using the Parabolized Navier-Stokes technique[3]. The computations have been performed in a novel rotating coordinate frame which rotates at the spin rate of the projectile[1]. The fluid flow relative to the rotating coordinate frame does not vary with time, allowing the steady (non-time varying) Navier-Stokes equations to be applied. The solution of the steady Navier-Stokes equations can be performed at a reasonable computational cost. In order to implement the rolling coordinate frame, the governing equations have been modified to include the effect of centrifugal and Coriolis forces. The steady thin-layer Navier-Stokes equations are shown below.

$$\frac{\partial E}{\partial \xi} + \frac{\partial F}{\partial \eta} + \frac{\partial G}{\partial \zeta} + S + H = \frac{\partial G_v}{\partial \zeta} + S_v \tag{4}$$

Here, E, F, and G are the inviscid flux vectors, G_v is the viscous flux vector, S and S_v are inviscid and viscous source terms due to the cylindrical coordinate formulation, and

H is the source term containing the Coriolis and centrifugal force terms which result from the rotating coordinate frame. Each of these matrices are functions of the dependent variables represented by the vector $q(\rho, \rho u, \rho v, \rho w, e)$, where ρ and e are the density and the total energy per unit volume, and u, v, and w, are the velocity components in axial, circumferential, and normal directions. The pressure, p, can be related to the dependent variables by applying the ideal gas law. The inviscid terms are shown below.

$$E = \frac{1}{J}\begin{bmatrix} \rho U \\ \rho u U + \xi_x p \\ \rho v U \\ \rho w U \\ (e+p)U \end{bmatrix} \quad F = \frac{1}{J}\begin{bmatrix} \rho V \\ \rho u V + \eta_x p \\ \rho v V + \eta_\theta p/r \\ \rho w V + \eta_r p \\ (e+p)V \end{bmatrix} \quad G = \frac{1}{J}\begin{bmatrix} \rho W \\ \rho u W + \zeta_x p \\ \rho v W + \zeta_\theta p/r \\ \rho w W + \zeta_r p \\ (e+p)W \end{bmatrix} \tag{5}$$

$$S = \frac{1}{Jr}\begin{bmatrix} \rho w \\ \rho u w \\ 2\rho v w \\ \rho(w^2 - v^2) \\ (e+p)w \end{bmatrix} \quad H = \frac{1}{J}\begin{bmatrix} 0 \\ 0 \\ 2\Omega\rho w \\ -2\Omega\rho v - \Omega^2 r\rho \\ -\Omega^2 r\rho v \end{bmatrix} \tag{6}$$

Further details regarding the governing equations can be found in Reference 1.

The thin-layer equations are solved using the Parabolized Navier-Stokes technique of Schiff and Steger[3]. Improvements to the technique have been made by Rai, et al.[4]. These improvements have increased the robustness and the efficiency of the code and allowed application to complex configurations such as finned projectiles. Following the approach of Schiff and Steger, the governing equations, which have been modified here to include the Coriolis and centrifugal force terms, are solved using a conservative, approximately factored, implicit finite-difference numerical algorithm as formulated by Beam and Warming[5]. A single calculation (one Mach number, one spin rate) required approximately one hour on a Cray-2 supercomputer.

IV. ENGINEERING ESTIMATION APPROACH

1. Estimation of the Roll Damping of a KE Fin

One approach for estimating the roll damping of a KE fin is to use a strip theory approach, breaking the fin planform into many small strips. Each strip is assumed to be a two-dimensional flat plate at angle of attack, where the local angle of attack is a function of the local circumferential velocity due to the spin and the axial component of the velocity. The roll moment is then determined by integrating the lift on each strip multiplied by the local moment arm. Note that sign of the roll moment will be negative since the roll moment opposes the spin. The roll damping moment, which is the variation in the roll moment with spin, can be determined by dividing the roll moment by the non-dimensional spin rate, since roll moment on the flat plate fin will be zero at zero spin rate. In the current approach, the lift on each strip is determined from linearized potential theory.

The resulting equation for the roll damping moment coefficient is shown below,

$$C_{l_p} = \frac{-16N_{fins}}{\pi\sqrt{M_\infty^2 - 1}} \int_{r_{root}/D}^{r_{tip}/D} \frac{c(r/D)}{D} \left(\frac{r}{D}\right)^2 d\left(\frac{r}{D}\right) \tag{7}$$

where N_{fins} is the number of fins, $c(r/D)$ is the local chord length at the nondimensional radial position r/D, and r_{root} and r_{tip} are the radial distances to the fin root and fin tip.

2. Estimation of the Roll Producing Moment on a Canted Fin

The approach used to estimate the roll producing moment on a canted fin parallels the approach used to compute the roll damping moment. Strip theory is again applied, and the fin is treated as a two-dimensional flat plate at angle of attack, where the angle of attack is the equal to the cant angle, δ. The roll producing moment is determined by integrating the lift on each strip multiplied by the local moment arm. As before, the lift on each strip is determined from linearized potential theory. The resulting integral expression for the roll producing moment coefficient is shown below.

$$C_{l_o} = \frac{16N_{fins}\delta}{\pi\sqrt{M_\infty^2 - 1}} \int_{r_{root}/D}^{r_{tip}/D} \frac{c(r/D)}{D} \left(\frac{r}{D}\right) d\left(\frac{r}{D}\right) \tag{8}$$

3. Estimation of the Roll Producing Moment on a Beveled Fin

The roll producing moment caused by the machined asymmetry on the trailing edge of the fin can be estimated using simple compressible flow theory. Since the trailing edge of the fin is machined at a constant slope, this region can be treated as an inverted wedge and the equations for Prandtl-Meyer flow can be applied to compute the pressure difference across on the trailing edge bevel. The roll producing moment can be computed by obtaining the product of the pressure difference, the bevel area, and the distance from the projectile axis to the centroid of the area. The roll producing moment coefficient is expressed below.

$$C_{l_o} = \frac{N_{fins}(\Delta p/p_\infty)AZ}{\frac{1}{2}\gamma M_\infty^2} \tag{9}$$

Here, A is the bevel area, Z is the distance from the projectile axis to the centroid of the area, γ is the ratio of specific heats, and $\Delta p/p_\infty$ is the pressure difference nondimensionalized by the freestream static pressure.

V. RESULTS

Computations have been performed to determine the following aerodynamic parameters which determine the roll characteristics of the three fin designs: the roll producing moment, the roll damping moment, and the equilibrium spin rate. The computations were performed over a range of Mach numbers (M = 3.0 to 5.0) and spin rates (0 to 15 degrees

per meter) for free-flight (sea-level) atmospheric conditions. In the computations, each fin design was mounted on a high L/D cone-cylinder forebody. The half angle of the conical nose was eight degrees. The results for each fin configuration are discussed separately in the flowing three sections.

1. Fin Configuration 1

Predictions of both the roll producing moment coefficient and roll damping moment coefficient as a function of Mach number are shown in Figures 4 and 5, respectively. Both the PNS predictions and the predictions made using the engineering estimation procedure show similar trends for both of the aerodynamic coefficients. Compared to the PNS computations, the engineering approach over-predicts the roll producing moment by up to 31 percent and roll damping moment by as much as 41 percent. This over-prediction results because of the approximations made in the engineering approach, which neglects effects such as three-dimensional flow effects, tip effects, and viscous effects. Further discussion is available in Reference 1.

The equilibrium spin rate as a function of Mach number is shown in Figure 6. As discussed previously, the equilibrium spin rate is defined as the spin rate for which the net roll moment is zero. Both approaches show an increase in the equilibrium spin rate with decreasing Mach number, though the spin rates predicted by the PNS approach show a greater variation with Mach number. (The trends shown here will be reversed if the spin rate is shown in revolutions per second (RPS) since the spin rate in RPS can be obtained by multiplying the spin rate in degrees per meter by a constant times the Mach number.) The maximum difference between the two predictions of equilibrium spin rate was 17 percent.

2. Fin Configuration 2

The second fin configuration, shown in Figure 2, has fin trailing edges which extend past the base of the projectile. The computational approach applied here cannot model this aspect of the configuration. Instead, the base of the projectile was extended so that the base of the projectile was aligned with the trailing edge of the fins. The modeled configuration, referred to as the extended body configuration, is shown schematically in Figure 7. The engineering approach, which is more flexible but more approximate, has been applied to both the actual configuration and the modeled configuration to assess the differences in the aerodynamic coefficients.

The prediction of the roll producing moment coefficient as a function of Mach number is shown in Figure 8. Again, the trend predicted by the computational and engineering approaches is similar. For the extended body configuration, the engineering approach over-predicts the roll producing moment coefficient by as much as 33 percent compared with the computational results. The engineering approach predicts that the roll producing moment of the actual configuration is four percent less than the extended body configuration, due to the decreased roll producing surface area of the actual configuration.

The predicted variation of the roll damping moment coefficient as a function of Mach number is shown in Figure 9. The engineering approach predicts very little difference in the roll damping of the actual and extended body configurations. Between Mach 4 and Mach 5, the computational and engineering approaches show similar variation with Mach number, though the magnitude of the engineering approach results is larger than the computational results. Below Mach 4, the computational results show less of an increase with decreasing Mach number than does the engineering approach. This behavior can be attributed to tip effects which become more pronounced at lower Mach numbers. The computational results exhibit this behavior because tip effects are inherently included. The engineering approach, as currently formulated, does not include tip effects.

Further evidence of the tip effects can be seen in Figure 10. This figure shows the local cumulative value of the roll damping moment coefficient as a function of Mach number for several intermediate axial locations on the fin. The local cumulative value of the roll damping moment coefficient is defined as the integrated value of the roll damping from the nose of the projectile to the stated axial location. The five curves shown correspond to axial locations which are 1.68, 2.79, 3.35, 3.91, and 4.48 calibers from the beginning of the fins. The axial location of 4.48 calibers corresponds to the trailing edge of the fins. As shown in Figure 11, the first three axial locations correspond to the axial locations where the fin has a delta planform; while the last two locations correspond to axial locations where the fin has reached it's maximum span. On the delta portion of the fin, the roll damping coefficient shows an asymptotic variation with Mach number. At the last two axial stations, the non-asymptotic behavior of the roll damping coefficient caused by tip effects is evident with the effect becoming more pronounced with increasing distance from the initial location where the fin reaches it's maximum span.

The equilibrium spin rate as a function of Mach number is shown in Figure 12. The computed results again show more of a variation with Mach number than does the engineering approach. Below Mach 4, the computed results show a change in the Mach number variation. This change is due to the decrease in the roll damping caused by tip effects. For the extended body configuration, the maximum difference between the predictions of equilibrium spin rate was 36 percent though the agreement in the vicinity of the launch velocity is much better. The engineering predictions show a 3.5 percent difference in equilibrium spin rate between the actual and extended body configurations.

At the time this report was written, 20 rounds with the second fin design had been fired through the Ballistic Research Laboratory Transonic Range[6]. The launch Mach number of the rounds varied between 2.7 and 5.0. The free-flight motion of the rounds was measured including the spin rates at two stations along the trajectory. Spin rates were measured using spin card arrays. Using the closed form solution[2] of the roll equation, a spin trajectory was fit through each of the rounds. Since rounds fired from a smooth-bore gun typically have nearly zero initial spin rate, the initial spin rate was assumed to be zero.

The comparison of the predicted and experimentally determined variation of the equilibrium spin rate with Mach number is shown in Figure 13. A fairly significant amount of scatter in the range data is observed. At this time, the source of the scatter has not been identified. It is thought that the scatter is real, since the equilibrium spin rate obtained

from the data reduction is close to the value measured at the second spin card array. It is unlikely that the measurement of the spin rate from the spin card array would completely account for the scatter. The PNS predictions fall within low end of the scatter of the experimental data and appear to follow the Mach number trend shown in the range data.

Figures 14 and 15 show the predictions of the roll producing and roll damping moment coefficients as a function of Mach number compared with the results obtained from the range firings. The computed roll producing moment coefficient falls within the scatter of the range data. The range data appear to show the same variation with Mach number exhibited by the computed results. The computed roll damping moment coefficient also falls within the scatter of the range results though the computed results do lie about 20 percent above the center of the range data scatter.

Roll trajectories were obtained using the computed aerodynamic coefficients and comparisons made with the range measurements obtained from the two spin card arrays. Six trajectories were computed corresponding to the six groups of launch Mach numbers. The comparisons of the computed and range measured spin rates at the second station are well represented by the previously presented plot of steady-state spin rate. The computed results at the first station, located at a position were the projectile had reached 60 to 70 percent of the steady-state roll rate, fell within the scatter of the range data. Sixty-five percent of the range data measurements at this location were within 10 percent of the computed value.

3. Fin Configuration 3

The third fin configuration resembles the second fin configuration except that the fin is canted to produce roll. The cant angle of the fin was not specified before the start of the computations; but rather, the computations were used to determine the cant angle for a desired range of the equilibrium spin rate, specified to be between 12 to 14 degrees per meter (about 60 to 70 revolutions per second at Mach 5).

Because the trailing edges of the fins overhang the base, the computational approach requires that the configuration be modeled as an extended body as was done for the second fin configuration.

In order to determine the fin cant angle which would produce the desired range of equilibrium spin rate, computations were performed for two different cant angles, 0.2 and 0.4 degrees. Predictions of the roll damping moment coefficient and slope of the roll producing moment coefficient with cant angle were obtained. Determination of these two coefficients then allowed the appropriate cant angle to be selected using Equations 1 - 3.

The predicted variation of the roll damping moment coefficient as a function of Mach number is shown in Figure 16. The predictions of the roll damping coefficient are similar to the values predicted for the second fin configuration, due to the similarity of the fin planforms. The difference between the computed roll damping coefficients of the second and third fin configurations varied between one and five percent. This difference, verified by computation, was mainly due to the trailing edge bevel, which was present on the second

fin configuration and not on the third fin configuration. The computed results also show essentially no variation in the roll damping due to cant angle. The engineering estimate of the roll damping for the third fin design is identical to the second.

The prediction of the slope of the roll producing moment coefficient with cant angle as a function of Mach number is shown in Figure 17. The computed results demonstrate that the roll producing moment coefficient varies linearly with cant angle over the range of cant angles examined. Compared with the computed results, the engineering estimate shows a 40 to 85 percent overprediction of the roll producing moment coefficient. The engineering predictions show less than a one percent difference in the roll producing moment between the actual configuration and the extended body configuration.

For this fin geometry, both the roll damping moment coefficient and the roll producing moment coefficient show a slowing in the rate of increase with decreasing Mach number due to tip effects. The roll producing moment coefficient for this configuration shows tip effects because the entire fin is a roll producing surface. On the second fin configuration this effect was absent since only a small length of the fin produces roll, and correspondingly, the area affected by tip effects is quite small.

Based on the computed results, it was determined that a cant angle of 0.4 degrees would yield the appropriate range of spin rate. The equilibrium spin rate as a function of Mach number for a cant angle of 0.4 degrees is shown in Figure 18. For this particular configuration, the computed results show a small decrease in the spin rate with decreasing Mach number, a trend which is somewhat different than that shown for the beveled fins. The PNS approach predicts a spin rate which is about 1.5 to 2.5 degrees per meter less than the engineering approach. The engineering approach shows no variation with Mach number. This is because in the engineering approach, both the roll producing moment coefficient and roll damping moment coefficient have the identical variation with Mach number, $\sqrt{M_\infty^2 - 1}$. Since the equilibrium spin rate is obtained from the ratio of these two coefficients, there should be no variation of the equilibrium spin rate with Mach number according to this simple theory. The engineering predictions show almost no difference in equilibrium spin rate between the actual and extended body configurations.

VI. CONCLUSION

The roll characteristics of three fin designs for a high length to diameter ratio kinetic energy projectile have been determined using a recently developed Computational Fluid Dynamics (CFD) approach. The roll characteristics of each of these designs have also been predicted using engineering estimation approaches.

The roll characteristics of the first two fin designs were predicted for a completely specified fin geometry. For the third fin design, the computational approach was applied to determine the appropriate cant angle to yield a desired range of equilibrium spin rate. Although Computational Fluid Dynamics approaches have previously provided useful information to the projectile designer, the current results represent the first CFD application within the US Army ballistics community where aspects of the projectile geometry were

determined using a three-dimensional Navier-Stokes computational approach.

For the second fin design, comparisons of the computed aerodynamic coefficients and equilibrium spin rates with the values obtained from the range firings show that the computational results fall within the scatter of the range data. These comparisons provide some degree of validation for the reported computational technique. From the standpoint of additional benchmarking of the computational approach, it would be desirable to have more accurately determined roll trajectories from the range firings. This might be accomplished by simply placing additional spin card arrays along the portion of the trajectory where the projectile is spinning up.

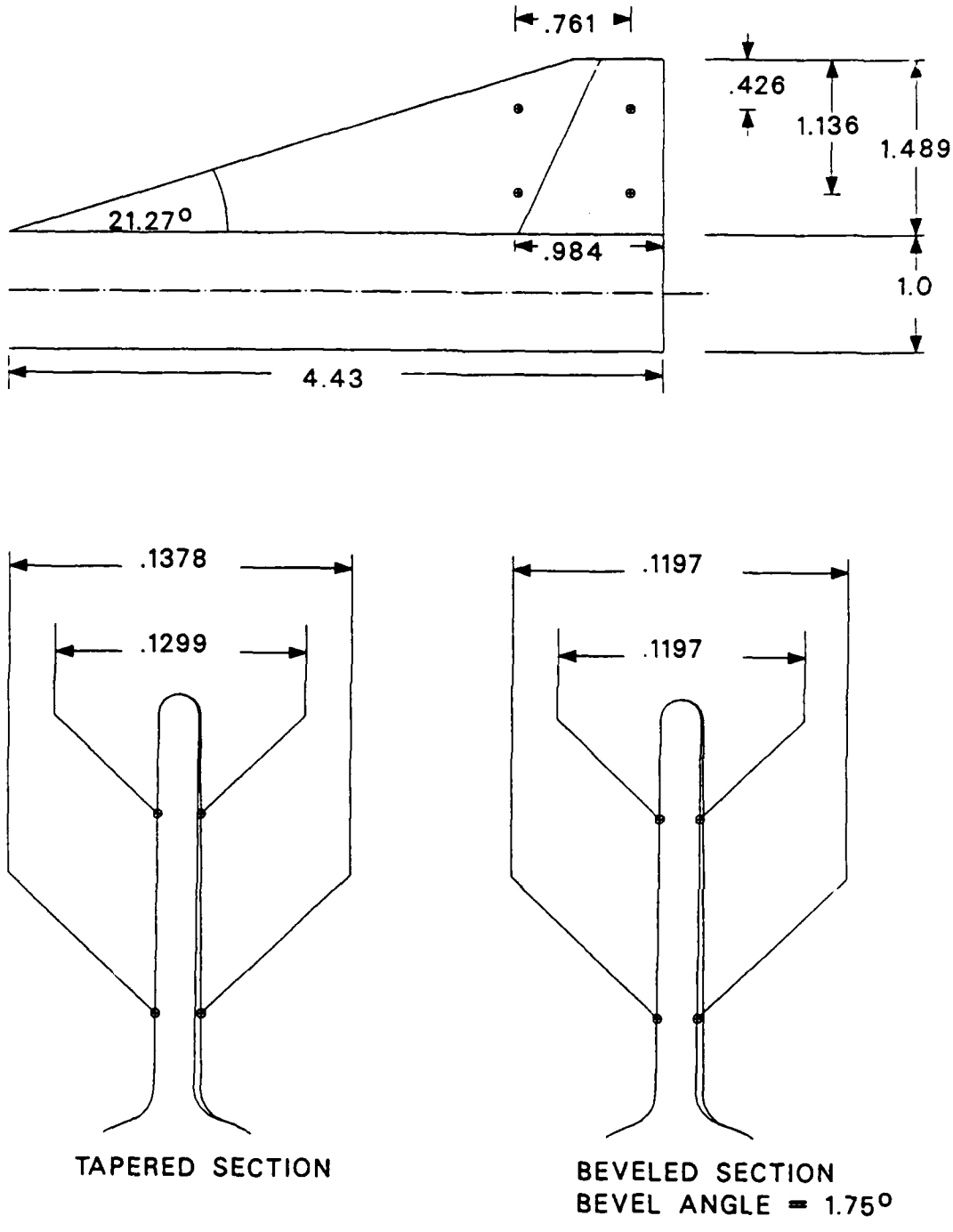

Figure 1. Schematic of fin design 1

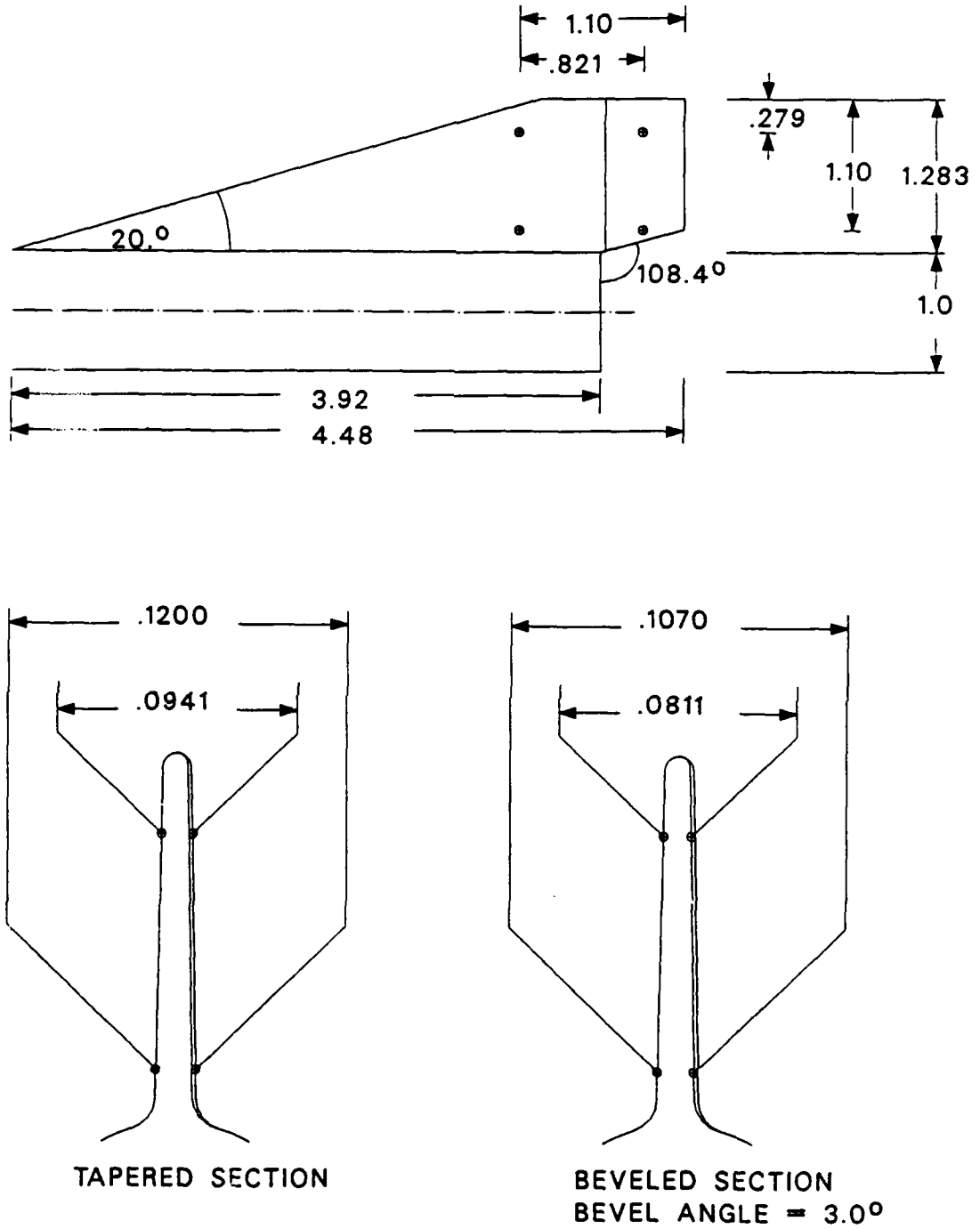

Figure 2. Schematic of fin design 2

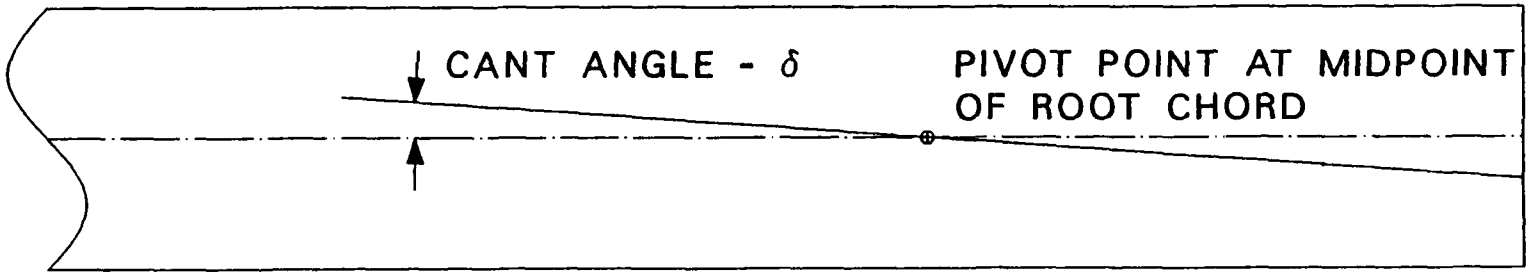

Figure 3. Schematic of fin design 3

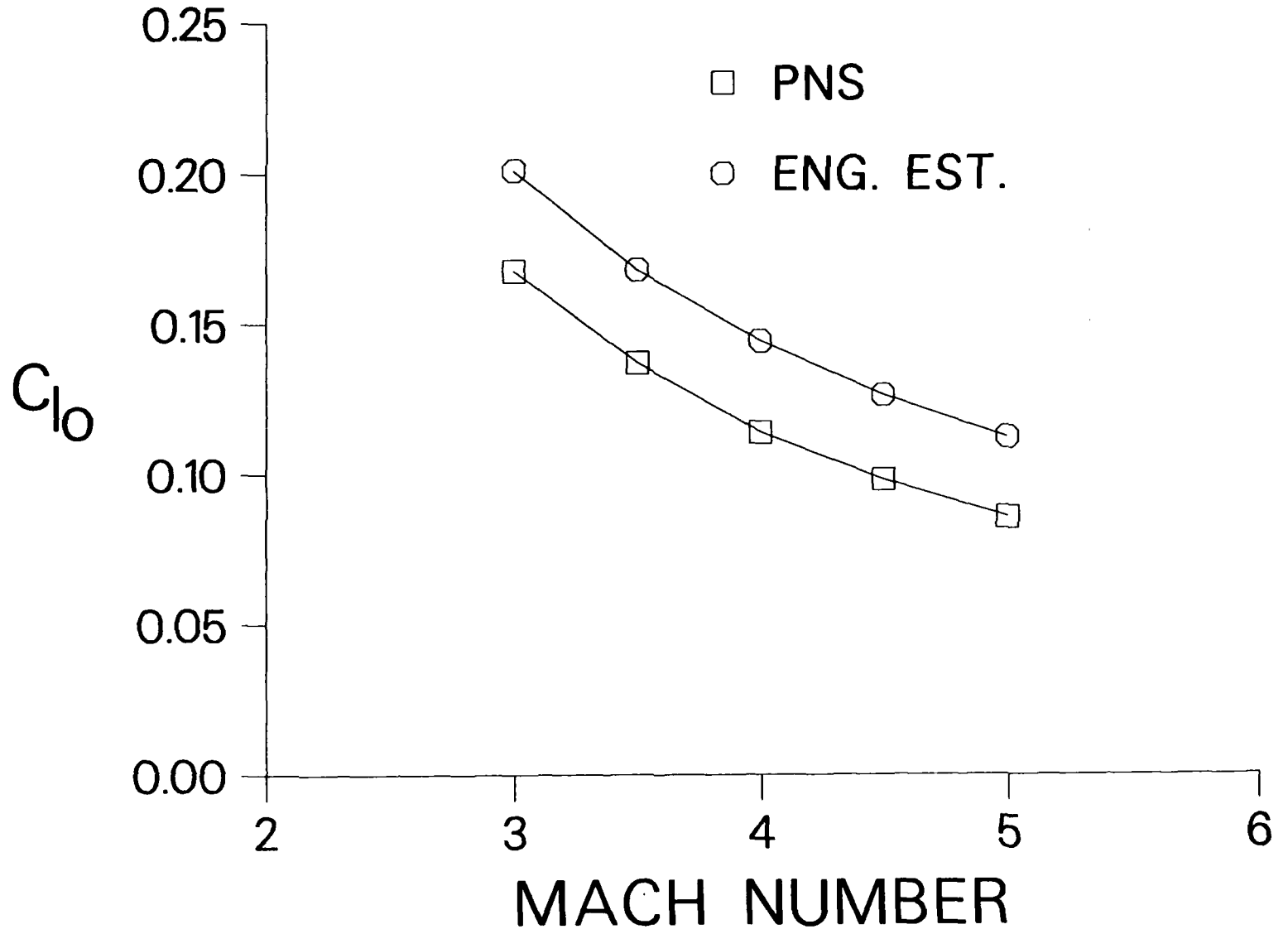

Figure 4. Variation of the roll producing moment coefficient with Mach number - Fin 1

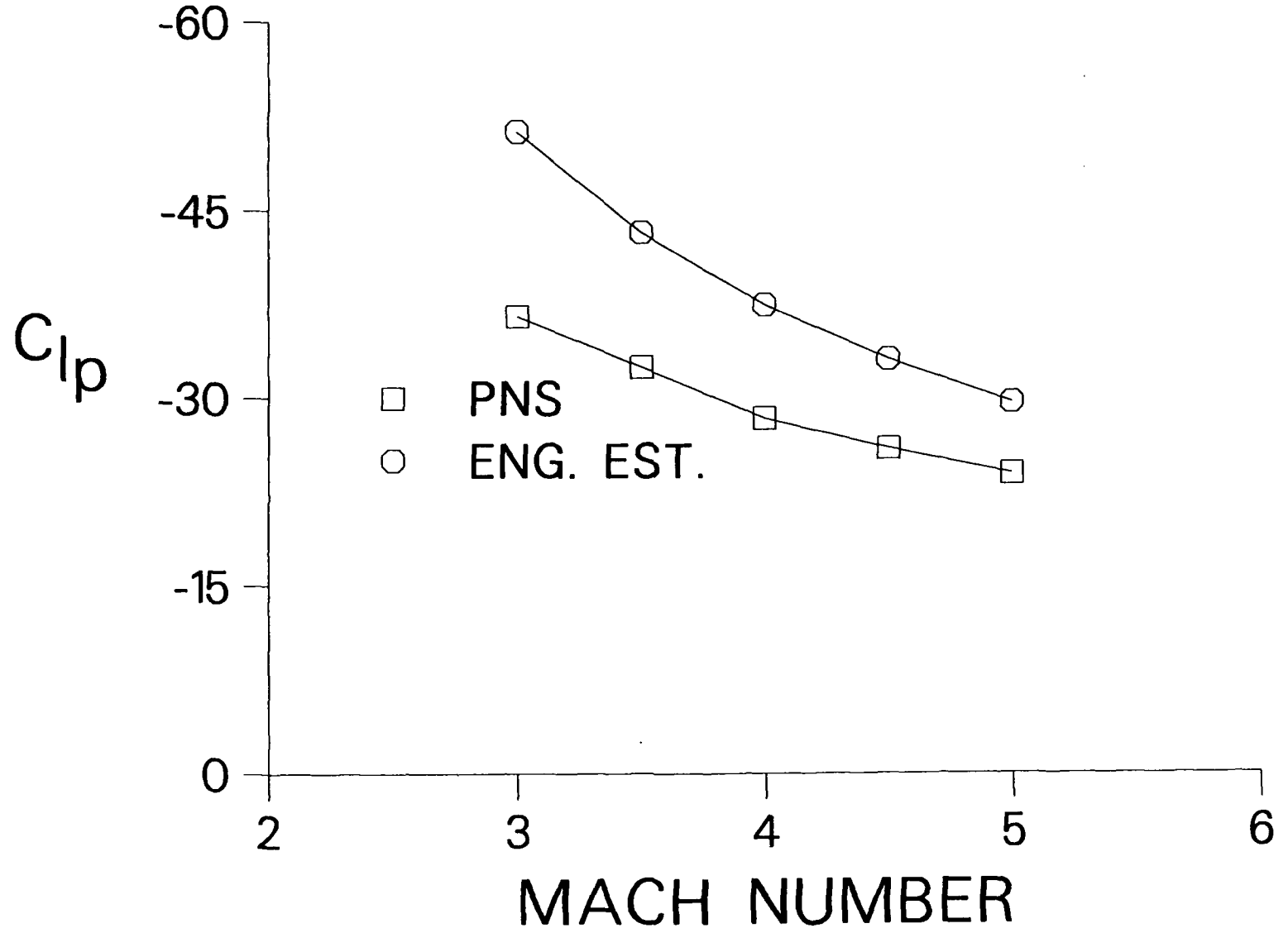

Figure 5. Variation of the roll damping moment coefficient with Mach number - Fin 1

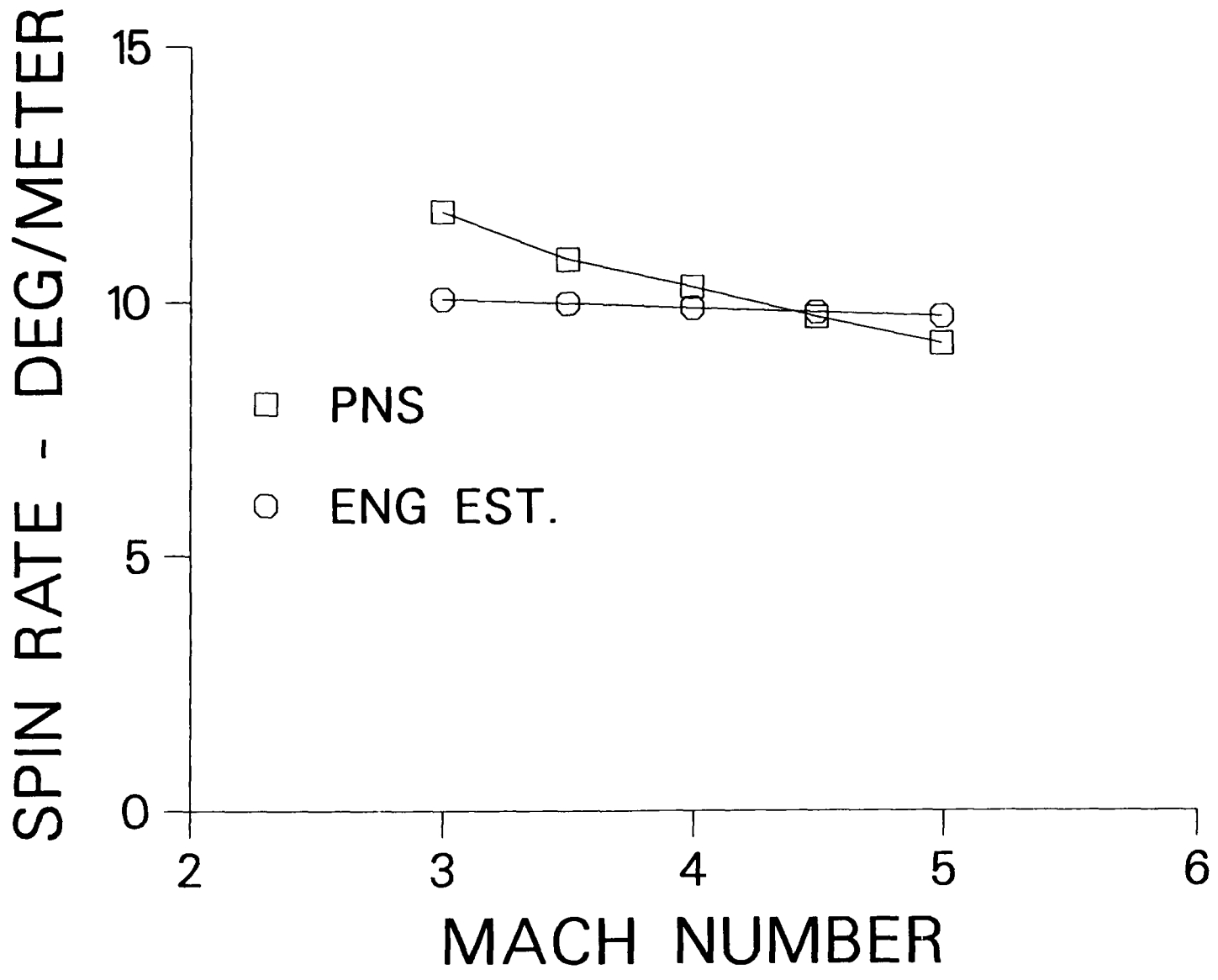

Figure 6. Variation of the equilibrium spin rate with Mach number - Fin 1

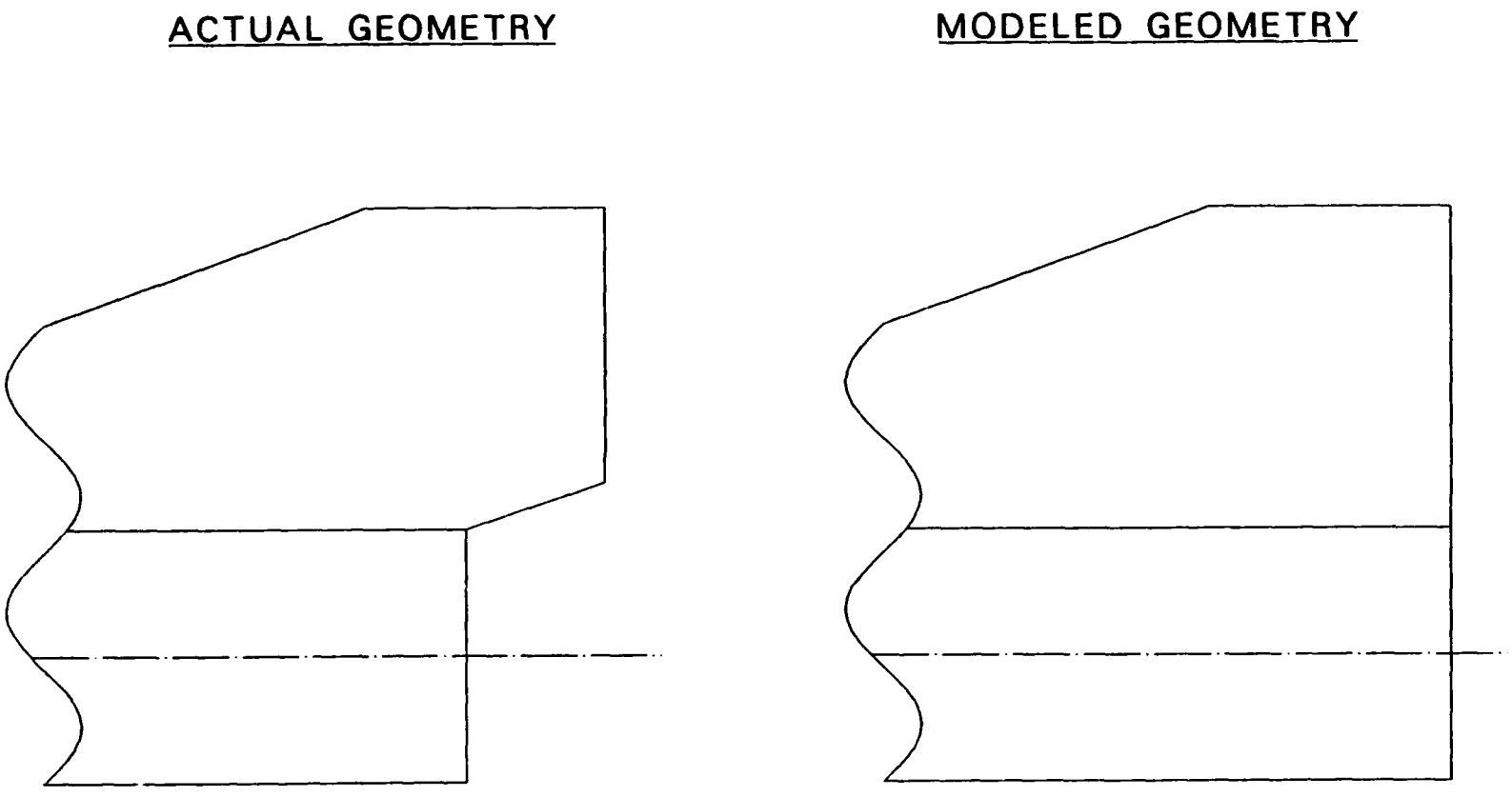

Figure 7. Schematic of actual and extended body configurations - Fin 2

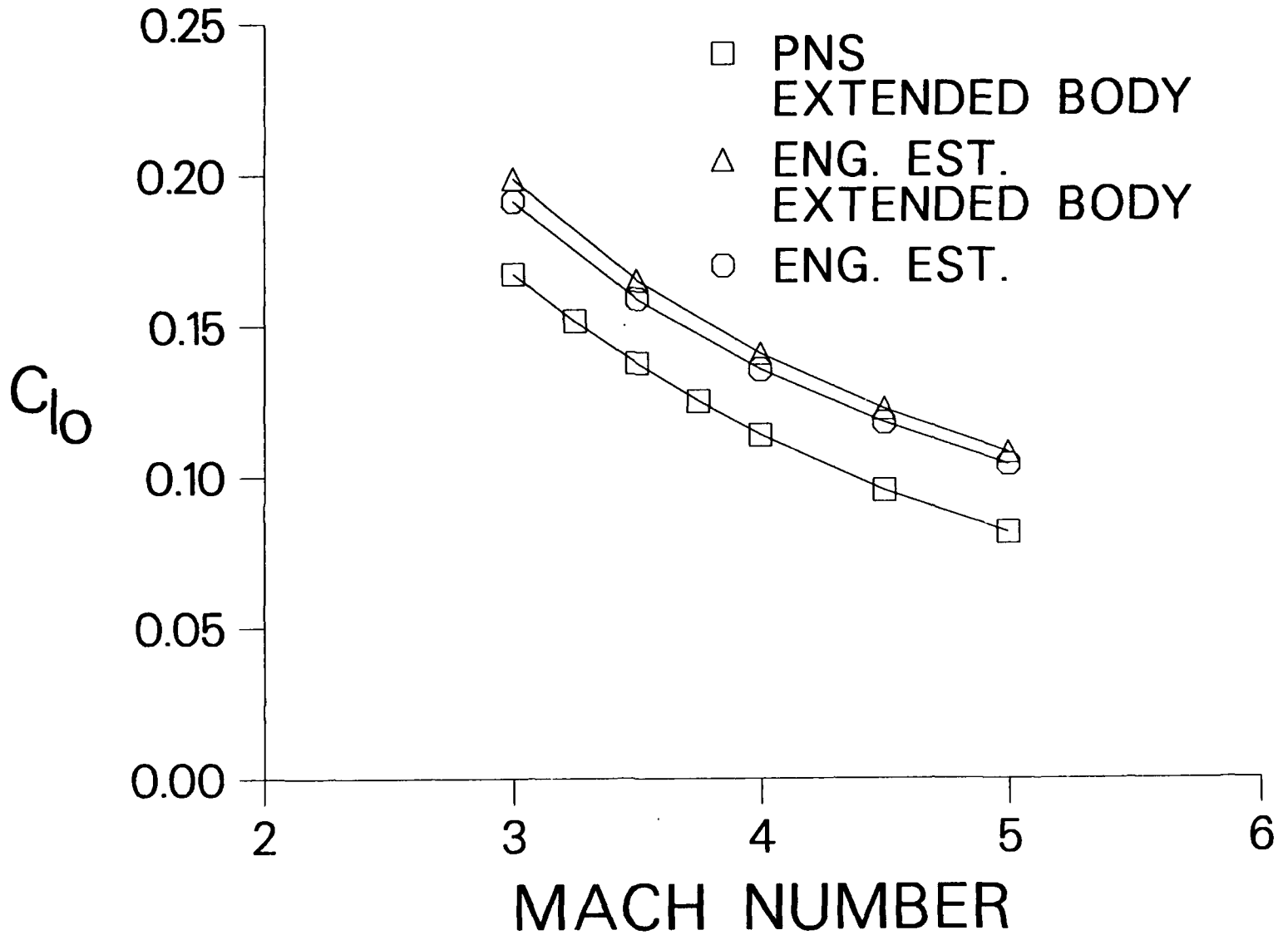

Figure 8. Variation of the roll producing moment coefficient with Mach number - Fin 2

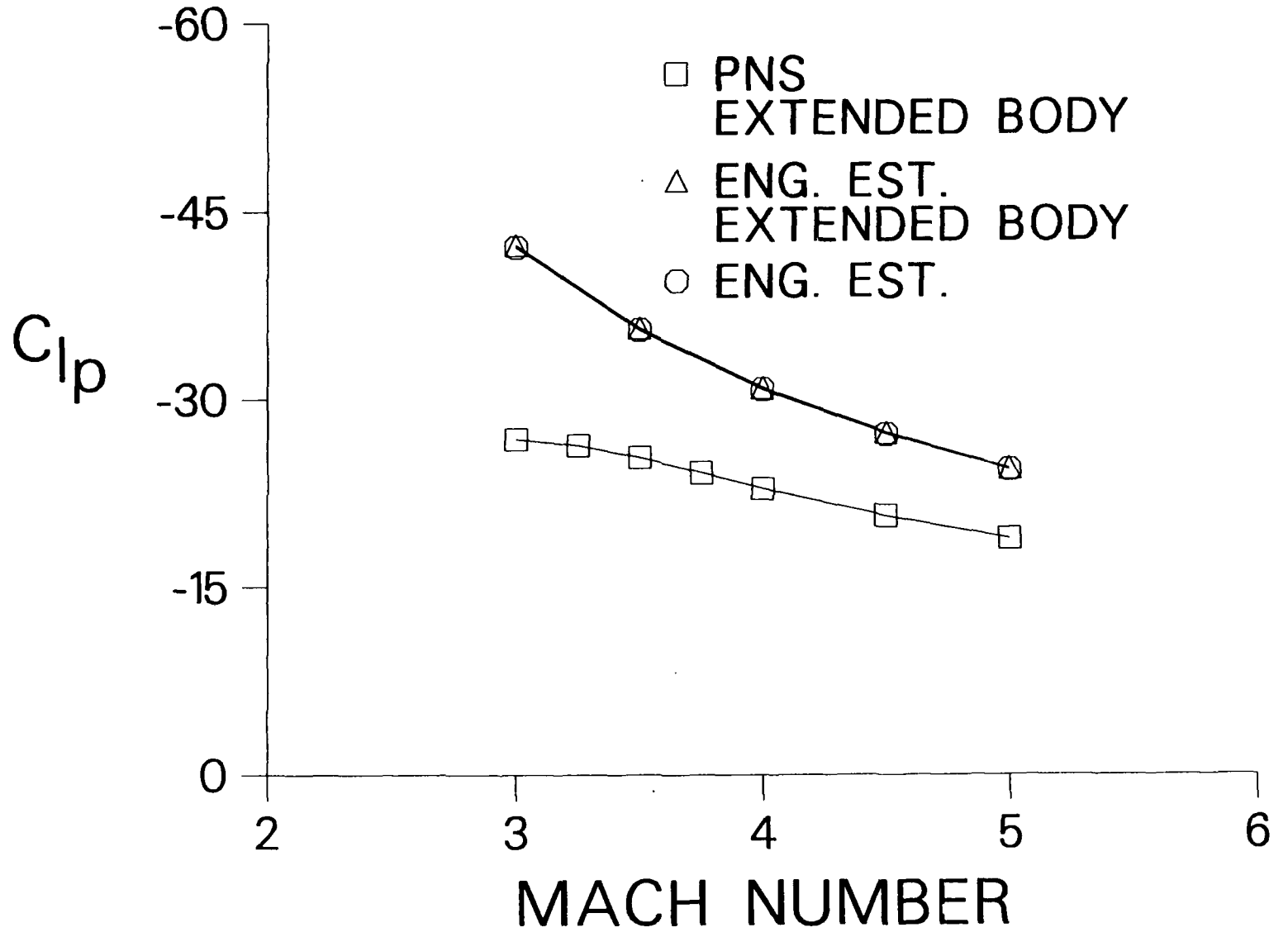

Figure 9. Variation of the roll damping moment coefficient with Mach number - Fin 2

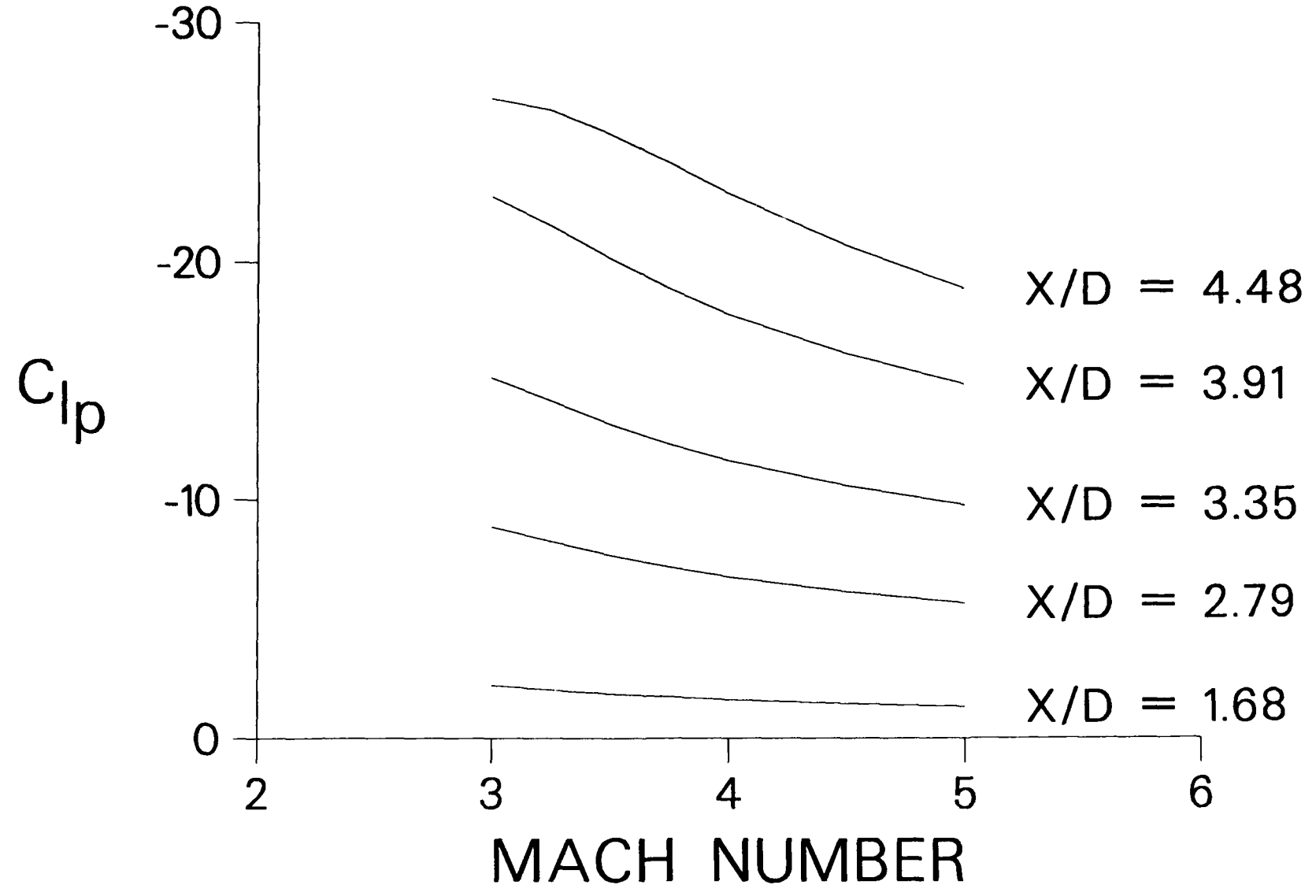

Figure 10. Variation of the local roll damping moment coefficient with Mach number for several axial locations - Fin 2

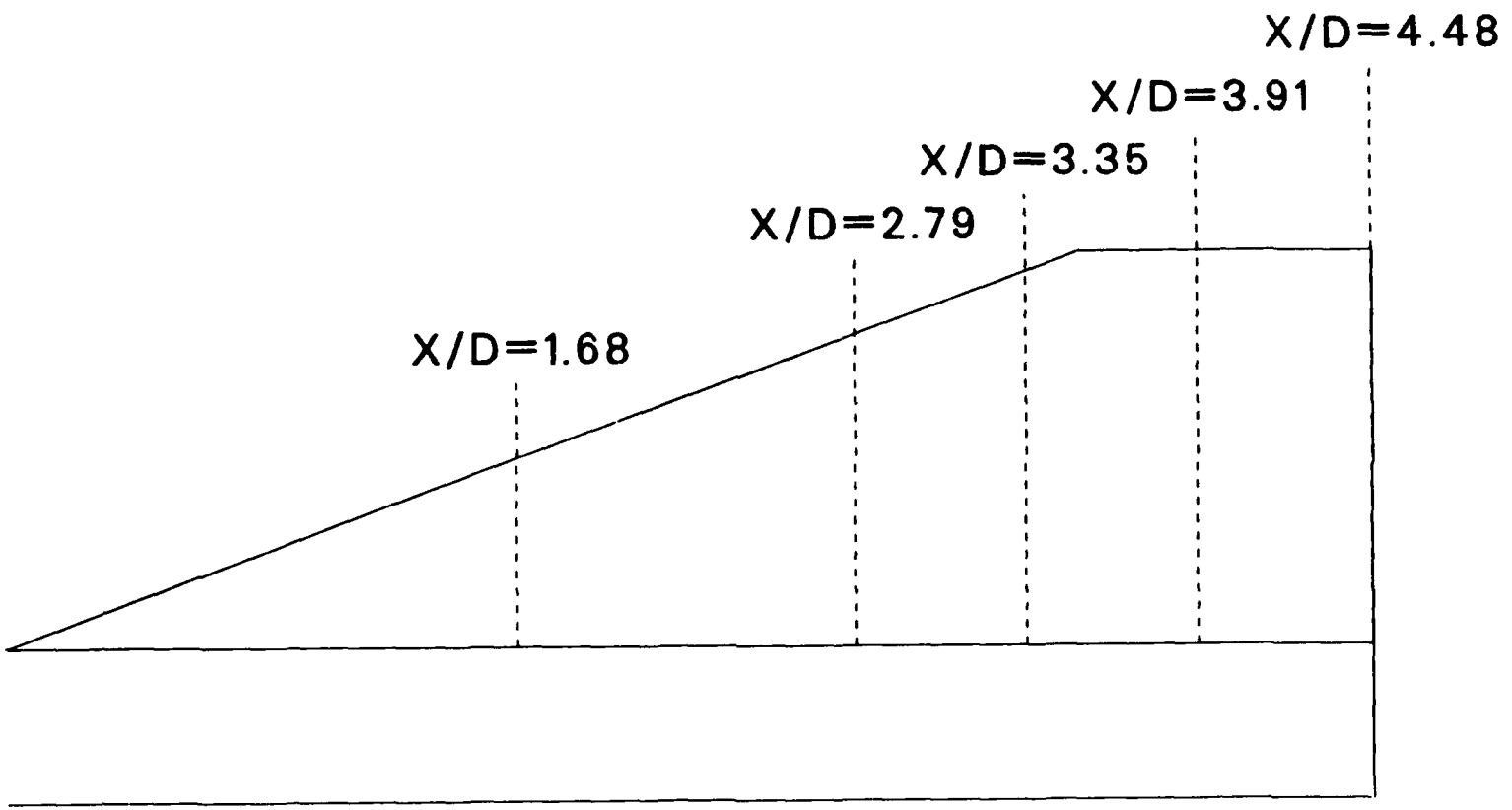

Figure 11. Locations of axial stations where local roll damping moment coefficient is examined

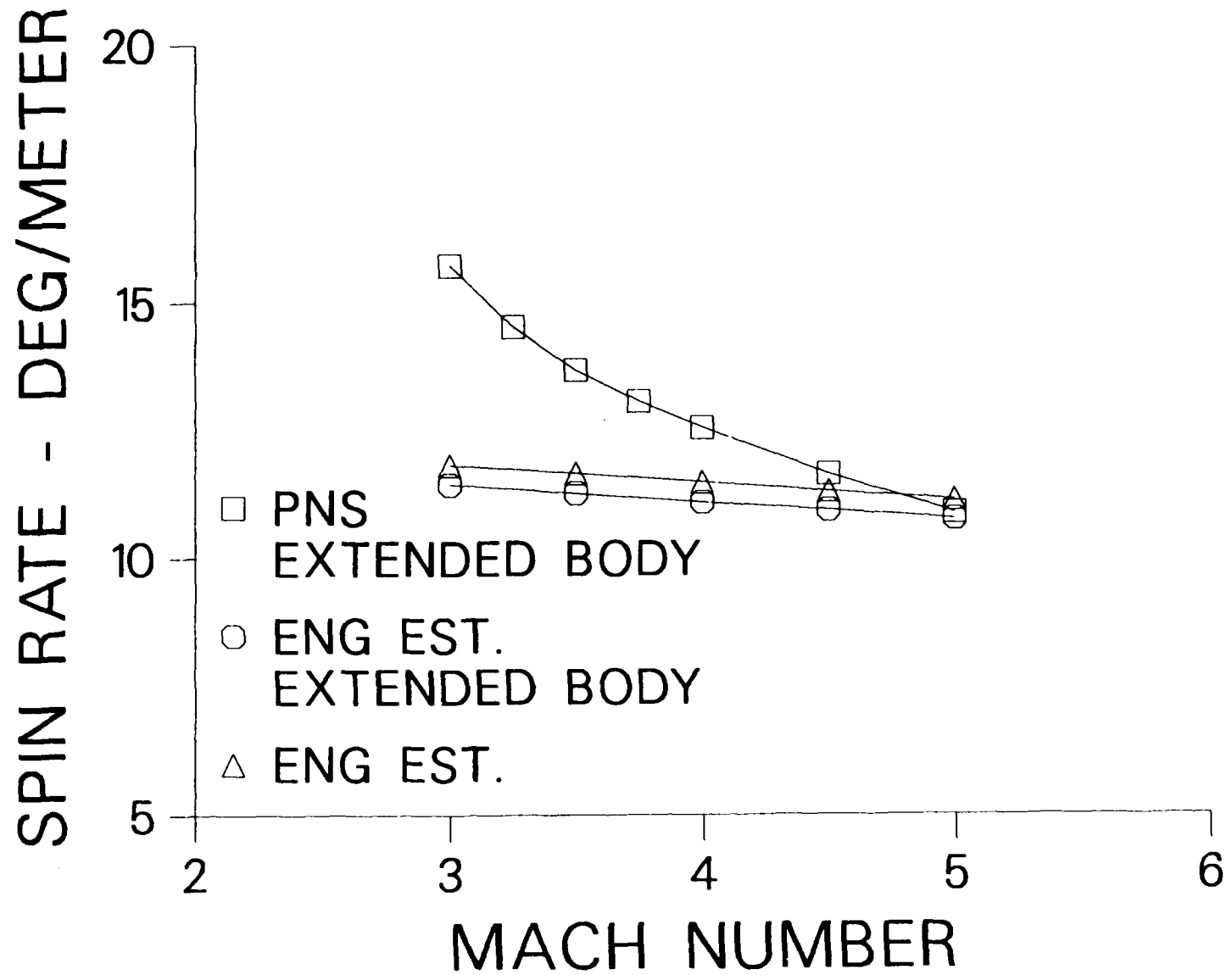

Figure 12. Variation of the equilibrium spin rate with Mach number - Fin 2

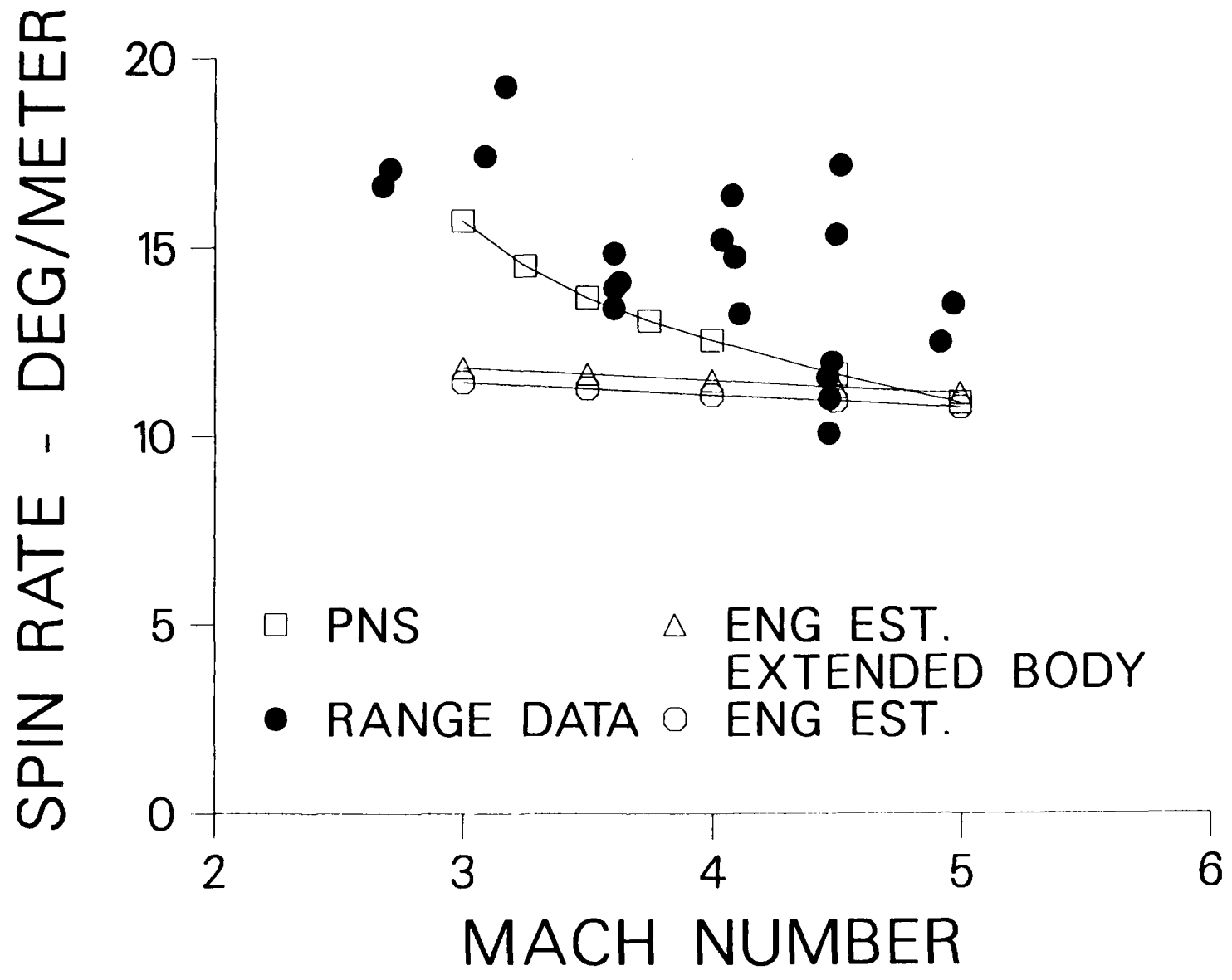

Figure 13. Predicted and measured variation of the equilibrium spin rate with Mach number - Fin 2

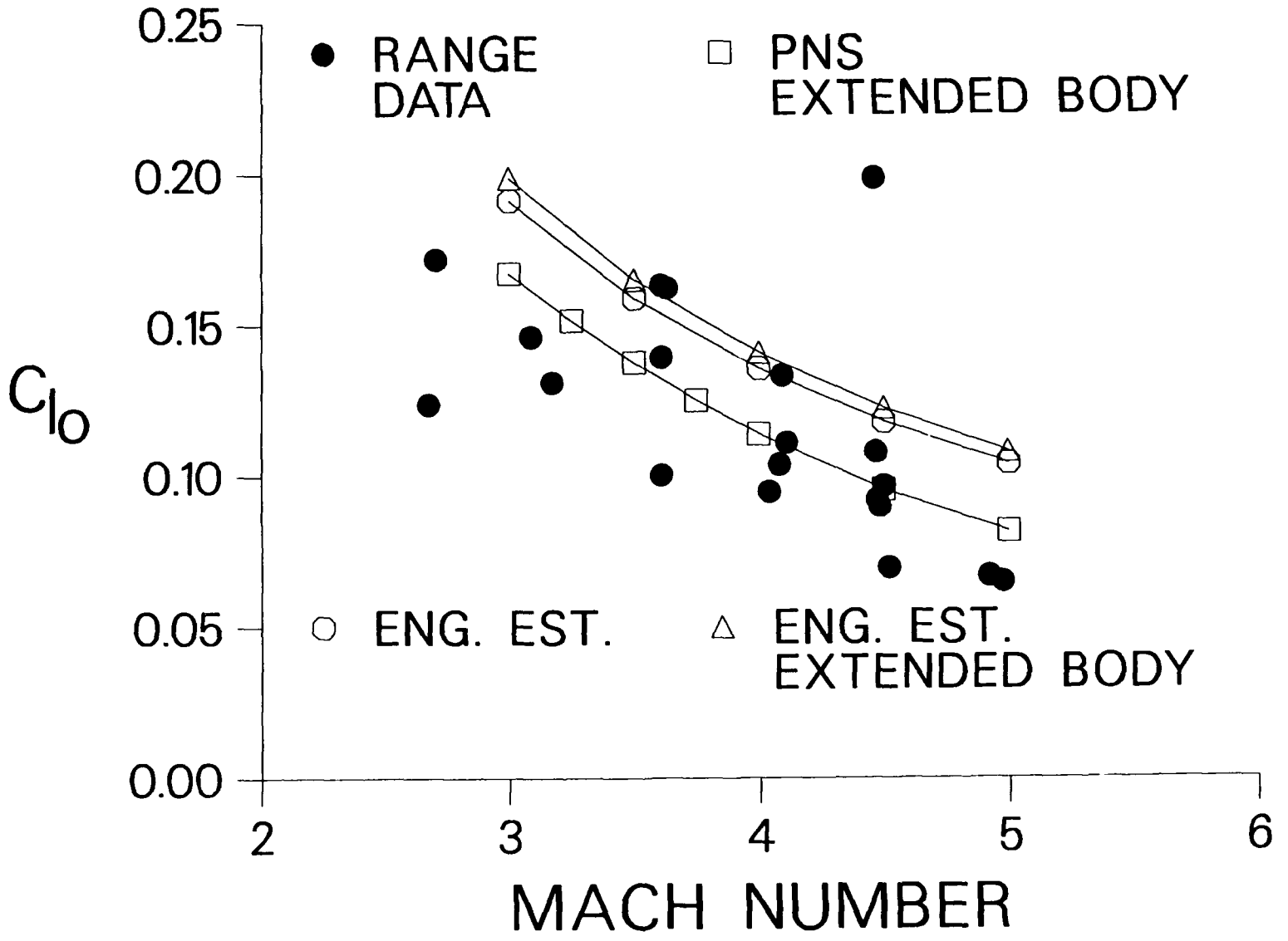

Figure 14. Predicted and measured variation of the roll producing moment coefficient with Mach number - Fin 2

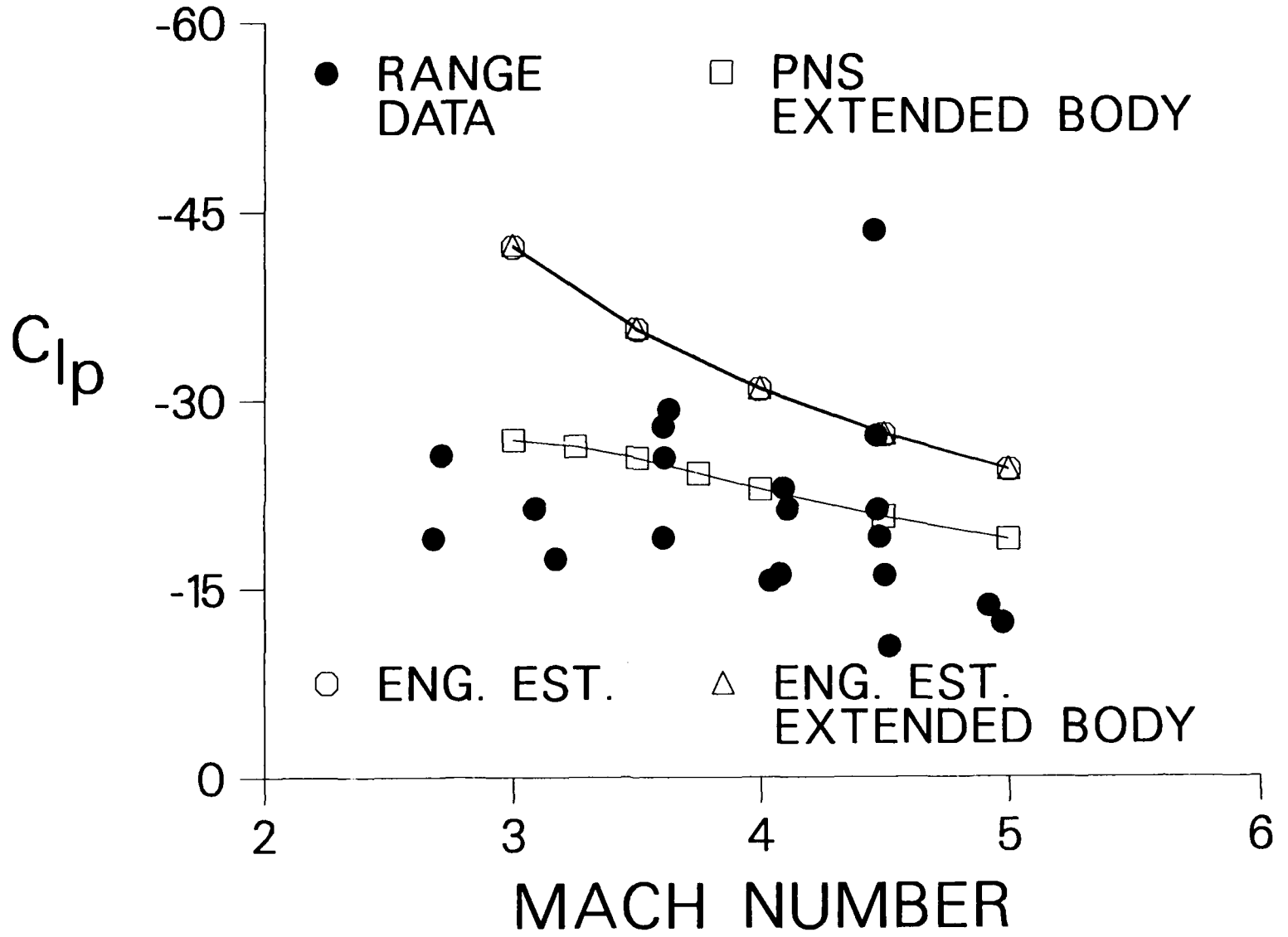

Figure 15. Predicted and measured variation of the roll damping moment coefficient with Mach number - Fin 2

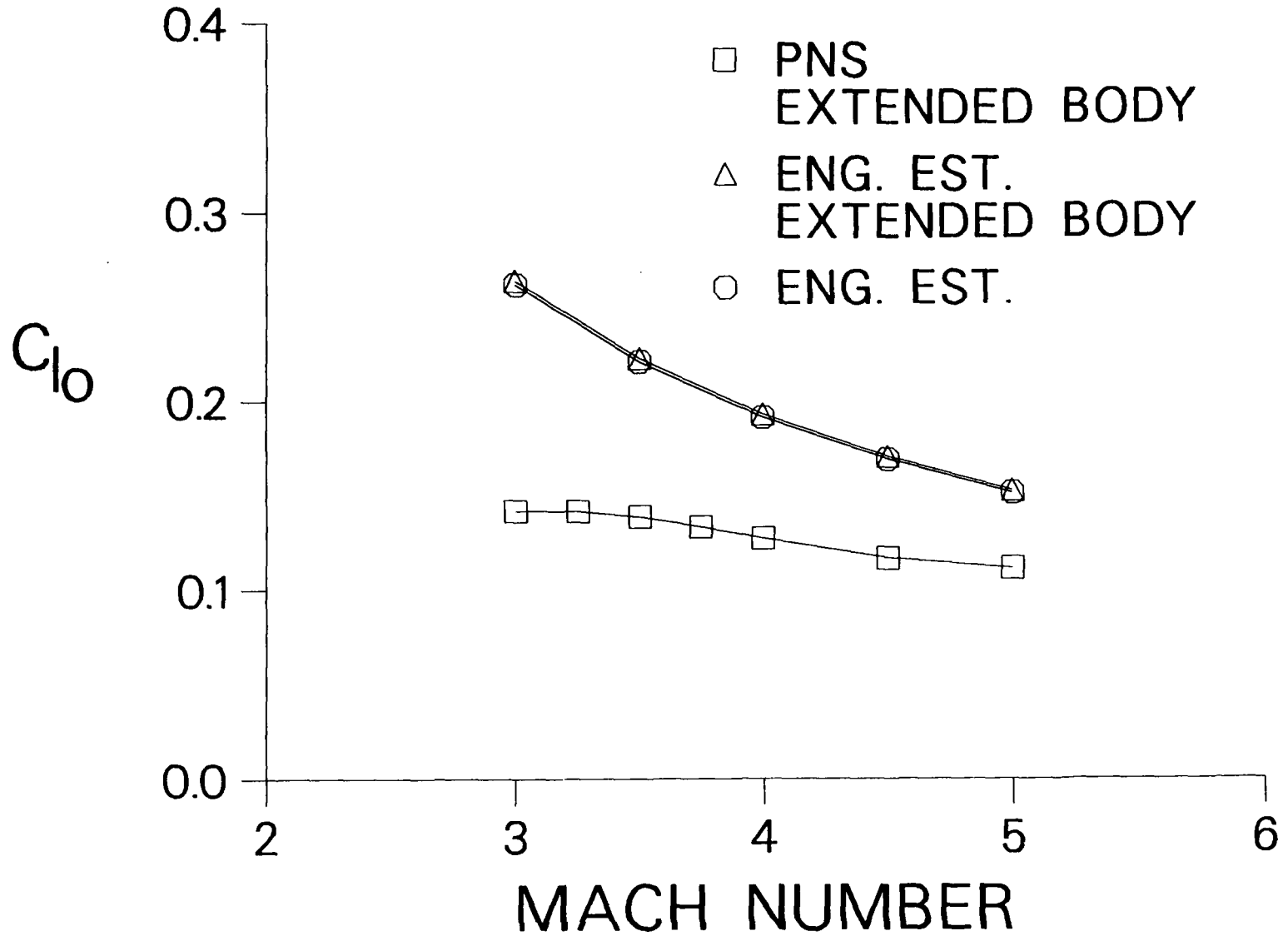

Figure 16. Variation of the roll damping moment coefficient with Mach number - Fin 3

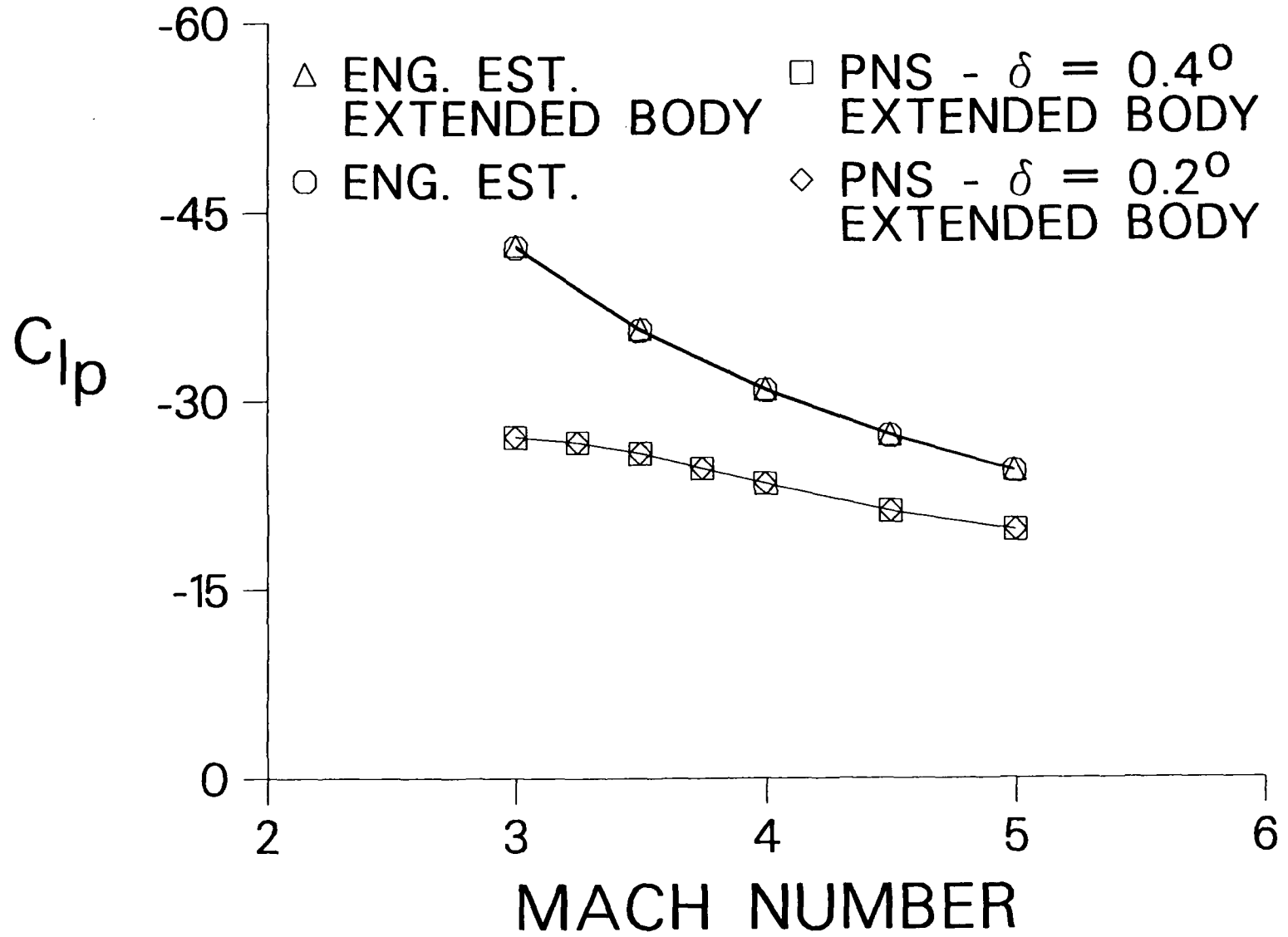

Figure 17. Slope of the roll producing moment coefficient with cant angle as a function of Mach number - Fin 3

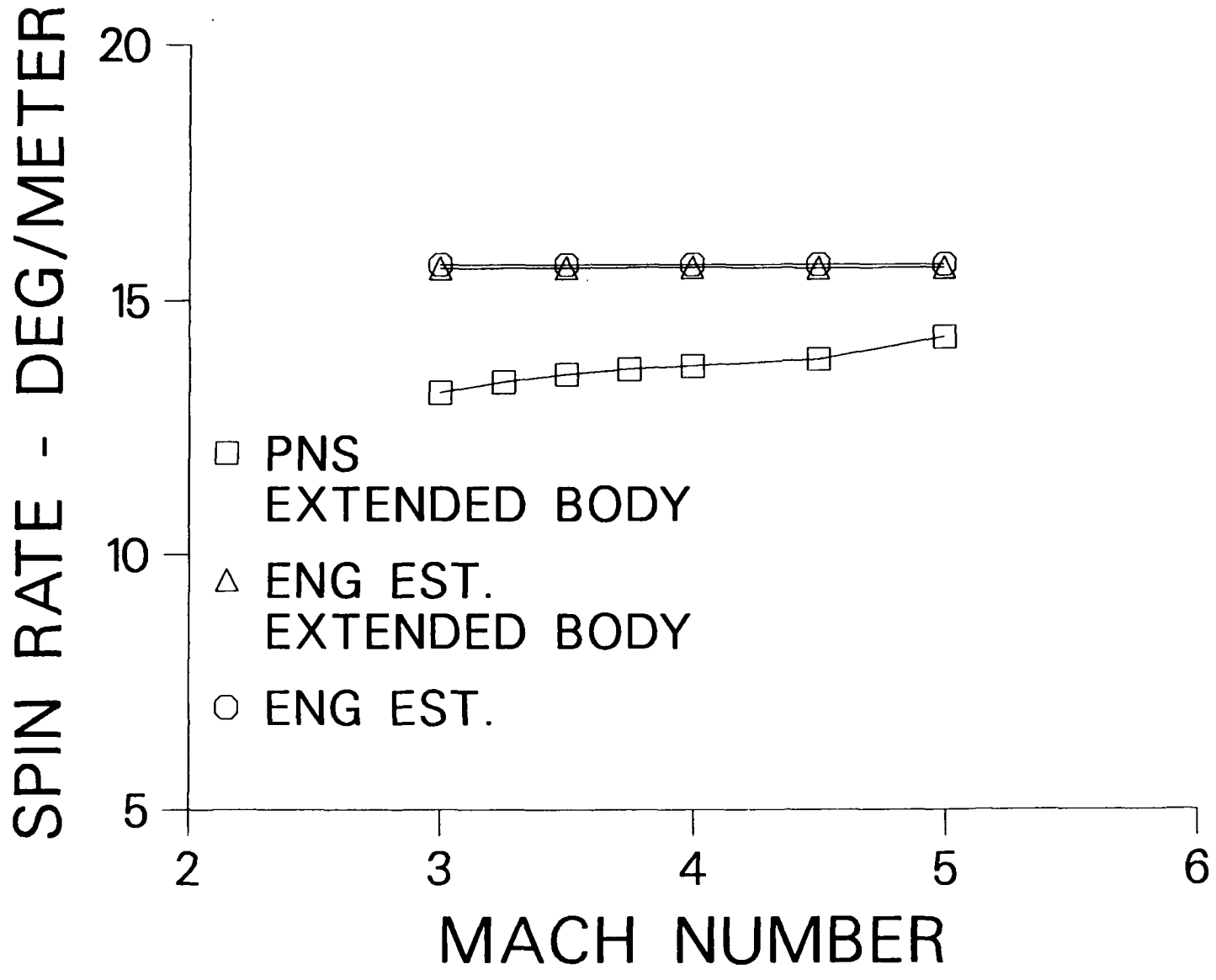

Figure 18. Variation of the equilibrium spin rate with Mach number, Cant angle = 0.4^o - Fin 3

References

1. Weinacht, P., and Sturek, W.B., "Computation of the Roll Characteristics of Finned Projectiles," U.S. Army Ballistic Research Laboratory, Aberdeen Proving Ground, Maryland, Technical Report BRL-TR-2931, June 1988.

2. Murphy, C.H., "Free Flight Motion of Symmetric Missiles," U.S. Army Ballistic Research Laboratory, Aberdeen Proving Ground, Maryland, Report No. 1216, July 1963. (AD A442757)

3. Schiff, L.B., and Steger, J.L., "Numerical Simulation of Steady Supersonic Viscous Flow," AIAA Journal, Vol. 18, No. 12, December 1980, pp. 1421-1430.

4. Rai, M.M., Chaussee, D.S., and Rizk, Y.M., "Calculation of Viscous Supersonic Flows over Finned Bodies," AIAA Paper No. 83-1667, Danvers, MA, July 1983.

5. Beam, R., and Warming, R.F., "An Implicit Factored Scheme for the Compressible Navier-Stokes Equations," AIAA Journal, Vol. 16, No. 4, 1978, pp. 85-129

6. Brandon, F.J., "Private Communication," U.S. Army Ballistic Research Laboratory, Aberdeen Proving Ground, Maryland

LIST OF SYMBOLS

a_∞	freestream speed of sound
A	area of trailing edge bevel
$c(r)$	local chord length of fin
C_l	roll moment coefficient
C_{l_o}	roll producing moment coefficient
C_{l_p}	roll damping moment coefficient
C_{l_δ}	slope of the roll producing moment coefficient with cant angle
D	projectile diameter
e	total energy per unit volume
E,F,G	flux vectors in transformed coordinates
G_v	viscous flux vector in transformed coordinates
H	source term resulting from rotating coordinate frame
I	moment of inertial
J	jacobian
M_∞	freestream Mach number
N_{fins}	number of fins
p	pressure, as used in thin-layer Navier-Stokes equations
p	spin rate, as used roll equations and aerodynamic coefficients
$\frac{pD}{V}$	nondimensional spin rate
p_∞	freestream static pressure
r	radial coordinate
S	inviscid source term resulting from the cylindrical coordinate formulation
S_{ref}	reference cross sectional area of projectile
S_v	viscous source term resulting from cylindrical coordinate formulation
t	time
u,v,w	axial, tangential, and normal velocity components of the Navier-Stokes equations
U,V,W	Contravariant velocities of the transformed Navier-Stokes equations
V	freestream velocity used to non-dimensionalize the spin rate and the aerodynamic coefficients
X_{LE}	distance from fin leading edge
Z	distance from projectile axis to centroid of area of trailing edge bevel

Greek Symbols

α(r)	local angle of attack
γ	ratio of specific heats
δ	fin cant angle
Δp	pressure difference across fin
ξ, η, ζ	transformed coordinates
ρ	density
ρ_∞	freestream density
Ω	spin rate of projectile

DISTRIBUTION LIST

No. Copies	Organization
12	Administrator Defense Technical Information Center ATTN: DTIC-DDA Cameron Station Alexandria, VA 22304-6145
1	HQDA (SARD-TR) Washington, DC 20310
1	Commander US Army Material Command ATTN: AMCDRA-ST 5001 Eisenhower Avenue Alexandria, VA 22333-0001
1	Commander US Army Laboratory Command ATTN: AMSLC-TD Adelphi, MD 20783-1145
1	Commander Armament R&D Center US Army AMCCOM ATTN: SMCAR-MSI Picatinny Arsenal, NJ 07806-5000
1	Commander Armament R&D Center US Army AMCCOM ATTN: SMCAR-TDC Picatinny Arsenal, NJ 07806-5000
1	Director Benet Weapons Laboratory Armament R&D Center US Army AMCCOM ATTN: SMCAR-LCB-TL Watervliet, NY 12189-4050
1	Commander US Army Armament, Munitions and Chemical Command ATTN: SMCAR-ESP-L Rock Island, IL 61299-7300
1	Commander US Army Aviation Systems Command ATTN: AMSAV-DACL 4300 Goodfellow Blvd St Louis, MO 63120-1798
1	Director US Army Aviation Research and Technology Activity Ames Research Center Moffett Field, CA 94035-1099
1	Commander US Army Missile Command ATTN: AMSMI-AS Redstone Arsenal, AL 35898-5000
1	Commander US Army Tank Automotive Command ATTN: AMSTA-DI Warren, MI 48090

DISTRIBUTION LIST

No. Copies	Organization
1	Director US Army TRADOC Analysis Cmd ATTN: ATAA-SL White Sands Missile Range, NM 88002-5502
1	Commandant US Army Infantry School ATTN: ATSH-CD-CSO-OR Fort Benning, GA 31905-5400
1	AFWL/SUL Kirtland AFB, NM 87117-6008
1	Air Force Armament Laboratory ATTN: AFATL/DLODL Eglin AFB, FL 32542-5000
2	Honeywell, INC. ATTN: Mark W. Swenson ATTN: Richard J. Buretta Mail Station MN48-3700 7225 Northland Drive Brooklyn Park, MN 55428
1	Honeywell, INC. ATTN: Mark Jones Mail Station MN48-2300 7225 Northland Drive Brooklyn Park, MN 55428
1	Arrow Technology Associates ATTN: Robert Whyte P.O. Box 4218 Burlington, VT 05491-0042
1	Honeywell, INC. ATTN: Fred Moynihan Defense Systems Division 5901 S. County Road 18 Edina, MN 55436
3	Commander Armament R&D Center US Army AMCCOM ATTN: SMCAR-CCH-W (A. Warnasch) SMCAR-CCH-W (K. Fehsal) SMCAR-CCH (J. DeLorenzo) Picatinny Arsenal, NJ 07806-5000
1	Commander Armament R&D Center US Army AMCCOM SMCAR-CCH-T ATTN: Saif Musalli Picatinny Arsenal, NJ 07806-5000
1	Commander Armament R&D Center US Army AMCCOM SMCAR-CCH-V ATTN: Ed Fennell Picatinny Arsenal, NJ 07806-5000
3	Commander Armament R&D Center US Army AMCCOM SMCAR-LCA-F ATTN: R. Kline J. Grau H. Hudgins Picatinny Arsenal, NJ 07806-5000
3	Commander Armament R&D Center US Army AMCCOM ATTN: AMCPM-TMA (Col. Mullen) AMCPM-TMA-105 (C. Kimker) AMCPM-TMA-120 (C. Roller) Picatinny Arsenal, NJ 07806-5000

DISTRIBUTION LIST

No. Copies	Organization	No. Copies	Organization
1	General Electric Co. ATTN: Dr. J.E. Daywitt Re-Entry Systems Operations 3198 Chestnut Street Philadelphia, PA 19101		

Aberdeen Proving Ground

Director, USAMSAA
ATTN: AMXSY-D
AMXSY-MP, H. Cohen

Commander, UASTECOM
ATTN: AMSTE-TO-F

Cdr, CRDC, AMCCOM
ATTN: SMCCR-MU
SMCCR-RSP-A
SMCCR-SPS-IL

USER EVALUATION SHEET/CHANGE OF ADDRESS

This laboratory undertakes a continuing effort to improve the quality of the reports it publishes. Your comments/answers below will aid us in our efforts.

1. Does this report satisfy a need? (Comment on purpose, related project, or other area of interest for which the report will be used.) _____

2. How, specifically, is the report being used? (Information source, design data, procedure, source of ideas, etc.) _____

3. Has the information in this report led to any quantitative savings as far as man-hours or dollars saved, operating costs avoided, or efficiencies achieved, etc? If so, please elaborate. _____

4. General Comments. What do you think should be changed to improve future reports? (Indicate changes to organization, technical content, format, etc.) _____

BRL Report Number _____ Division Symbol _____

Check here if desire to be removed from distribution list. ____

Check here for address change. ____

Current address: Organization _____
Address _____

----------FOLD AND TAPE CLOSED----------

Director
U.S. Army Ballistic Research Laboratory
ATTN: SLCBR-DD-T(NEI)
Aberdeen Proving Ground, MD 21005-5066

OFFICIAL BUSINESS
PENALTY FOR PRIVATE USE $300

BUSINESS REPLY LABEL
FIRST CLASS PERMIT NO. 12062 WASHINGTON D.C.
POSTAGE WILL BE PAID BY DEPARTMENT OF THE ARMY

NO POSTAGE NECESSARY IF MAILED IN THE UNITED STATES

Director
U.S. Army Ballistic Research Laboratory
ATTN: SLCBR-DD-T(NEI)
Aberdeen Proving Ground, MD 21005-9989